THE JOURNAL OF PHYSICAL CHEMISTRY C
A JOURNAL OF THE AMERICAN CHEMICAL SOCIETY

pubs.acs.org/JPCC

Article

Superatom Molecular Orbitals of Li@C_{60}: Effects of the Li Position and the Substrate

Artem V. Kuklin,* Rahul Suresh, Konoha Shimizu, Yoichi Yamada,* and Hans Ågren

Cite This: *J. Phys. Chem. C* 2022, 126, 15891−15898

Read Online

ACCESS | Metrics & More | Article Recommendations | Supporting Information

ABSTRACT: Understanding the character of superatom molecular orbitals (SAMOs) of fullerenes, especially those of the endohedral fullerenes, can potentially facilitate the utility of these molecules in organic electronics beyond conventional limits. However, the detailed nature of SAMOs in molecular films on substrates has yet to be unraveled. Using density functional theory, we investigate the wavefunction distributions and electronic structures of SAMO states of a Li@C_{60} monolayer in dependence on the position of Li within the cage and the type of substrate species. We find that the characteristics of the SAMOs in terms of shape and energy are quite sensitive to the Li position due to different charge redistributions. The substrate affects the intermolecular distances in the Li@C_{60} films and modifies the widths and dispersion of the SAMO bands while retaining energetics similar to that of the isolated Li@C_{60} monolayer. The substrate also affects the SAMO effective masses, making it possible to tune them via substrate-induced interaction. A properly chosen substrate can so be beneficial for Li confinement and SAMO stability, reflecting the molecule−substrate interaction and the charge transfer at the interface. These findings provide insights into the design and engineering of SAMOs of molecular films.

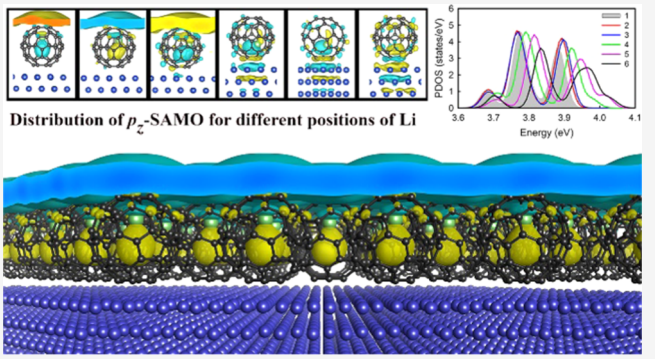

INTRODUCTION

Fullerene,[1] one of the most vital molecules in the field of organic electronics, has been proposed to be a good candidate for capturing individual atoms[2−4] and small clusters,[5−7] resulting in new exciting electronic properties and potential applications. Among the endohedral fullerenes, molecular materials based on Li@C_{60}[8−10] remain extremely interesting and promising for applications in nanotechnology. The discovery of nearly free electron (NFE) bands in empty states of C_{60} constitutes one of the most significant achievements in this area in recent years, suggesting enhancement of transport properties of fullerenes. Though the concept of diffuse empty states was defined already in 1991 by Martins et al. and Jost et al.,[11,12] the idea of superatom molecular orbitals (SAMOs) was introduced first in the context of C_{60},[13] based on results from scanning tunneling microscopy (STM) and density functional theory (DFT), and in particular, with the observation of delocalized SAMO states. Later, utilizing two-photon photoemission and STM techniques, SAMO states were confirmed at ∼3.3[14] and ∼3.63 eV[15] for s-SAMOs depending on the used substrate. It has been found that the spherical harmonic distribution induced by the C_{60} cage potential is responsible for the binding in SAMO states. Subsequently, their stability and long-lived nature were explained by many-body perturbation theory calculations of the quasiparticle decay times.[16] SAMO states have been proposed as ideal media for charge separation due to their diffuse character resulting in extremely weak electron−phonon (e−ph) interaction, so being a "phonon bottleneck" for hot electron cooling.[17]

One of the main challenges in C_{60} SAMO applications is the relatively high energy of SAMOs with respect to the Fermi level. Endohedral doping of C_{60} with Li has been proposed as a promising way for lowering the SAMO energy in Li@C_{60} compared to C_{60}—a 1.6 eV energy downshift of the s-SAMO was predicted in ref 18. It has also been found that due to the presence of Li inside the cage, symmetry is broken with asymmetrical spatial distributions of the superatom orbitals.[19]

SAMOs of isolated endohedral C_{60} molecules have been rather widely studied, while SAMOs of adsorbed molecules, especially in monolayer form, were not characterized until our recent report[20] in spite of their importance in practical applications.[17,21] Implementation of fullerenes into a real nanodevice always assumes interactions with a substrate, which can significantly change their electronic properties. For adsorbed molecules, a sizable interaction of SAMOs between adjacent molecules is important to realize a delocalized band

Received: March 27, 2022
Revised: August 27, 2022
Published: September 8, 2022

and so to make the system suitable for electron transport. Previously, it was challenging to produce ensembles of Li@C_{60} molecules with uniform adsorption geometry due to their considerable reactivity. However, recently, we used the weakly bonded $[Li^+@C_{60}]NTf_2^-$ salt to produce a Li@C_{60} monolayer on Cu(111), which contained an unprecedently large amount of Li@C_{60} molecules in a monolayer form.[20] Utilizing a state-of-art STM technique and first-principles calculations, we directly visualized the delocalized states produced by the p_z-SAMOs of the Li@C_{60} monolayer adsorbed on the Cu(111) surface. It has also been shown that there is a gap in the alteration of SAMOs depending on the Li position, which can be tuned by STM.[22] However, the surface effect has still remained unclear.

Here, using first-principles calculations, we calculate the SAMO wavefunctions of endohedral doped Li@C_{60} on pristine Cu(111) and Au(111) crystal surfaces and for different Li positions to reveal how the shape and the energy of SAMOs are determined. It is demonstrated that the substrate affects mainly the dispersion of SAMOs through the molecule–substrate interaction and that it changes the molecular ordering and Li confinement, while the effect on the energy of the SAMOs is minor. On the other hand, the Li position significantly changes the energy of the SAMO levels and affects the shape of their wavefunctions.

THEORETICAL METHODS

To realize the model as closely as possible to the real material, one has to utilize periodic boundary conditions, which were previously applied also in calculations of two-dimensional (2D) C_{60} arrays.[23] Here, we employed density functional theory (DFT) calculations with plane-wave basis sets using the D3-corrected[24] Perdew–Burke–Ernzerhof (PBE) exchange functional[25] in the form implemented in the Vienna Ab initio Simulation Package (VASP).[26,27] We used the projector augmented wave (PAW)[28] method and a 450 eV cutoff energy of the plane-wave basis set. The Monkhorst–Pack scheme[29] was used to sample the first Brillouin zone (BZ) by $6 \times 6 \times 1$ k-points. The convergence tolerances of forces and electronic minimizations were 10^{-2} eV/Å and 10^{-5} eV, respectively. The vacuum region was set to at least ∼12 Å to avoid any spurious interaction in the z-direction. Visualization for Electronic and Structural Analysis (VESTA) software[30] was utilized to plot atomic structures and isosurfaces. The "vaspkit" code was employed for postprocessing the results.[31]

RESULTS AND DISCUSSION

A well-ordered lattice of close-packed C_{60} and Li@C_{60} monolayers can be formed on the 4×4 Cu(111) superstructure. The calculated unit cell of bulk Cu (3.629 Å), which perfectly coincides with experimental data (3.613 Å)[32] was used to construct a 4×4 Cu(111) slab composed of 96 Cu atoms in six layers. Two bottom layers were fixed to represent a transition to copper bulk parameters. Abundant experimental and theoretical data propose that Li@C_{60}, as well as C_{60}, adsorb on the Cu(111) surface on hollow sites with a threefold symmetry hexagonal face.[33] Therefore, we placed Li@C_{60} on the 4×4 Cu(111) surface (Figure 1a) above the hcp sites. Electronic structure calculations were carried out for six positions of Li inside the C_{60} cage (Figure 1b). We found that Li in the top position (1), just below the top hexagon, is 0.13 eV energetically favorable compared to the bottom Li location (6), something that can be referred to as the Coulombic repulsion between the positive Li ion and the Cu slab and that it is displaced from the cage center by as much as 1.54 Å. Because of this, the Li ion inside C_{60} on the copper surface resides mostly within the upper hemisphere even at room temperature, as confirmed by ab initio molecular dynamics simulations,[20] making it easily accessible by the STM technique.[20,22]

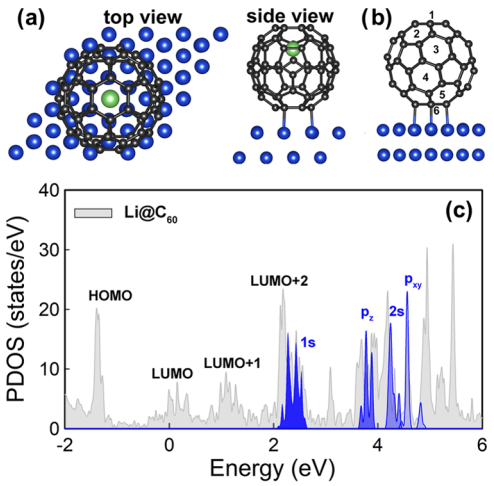

Figure 1. (a) Top and side views of equilibrium geometry of Li@C_{60} on Cu(111). (b) Six positions of Li inside the C_{60} cage. (c) Density of states of Li@C_{60}/Cu(111) projected on Li@C_{60} (gray filling) and SAMO states (blue fillings). The SAMO states are multiplied by a factor of 3 to guide the eye. The Fermi level is set to 0 eV.

The projected density of states (PDOS) of the SAMOs are determined by employing the electronic structure calculations and are shown in Figure 1c. The lowest energy of the 1s-SAMO has the same energy as that of the lowest unoccupied molecular orbital (LUMO) + 2 state. In contrast to C_{60}, where the 1s-SAMO is located above LUMO + 3,[18] the presence of Li inside the shell lowers the 1s-SAMO to the LUMO + 2 region. Previously, we have reported that the LUMO + 2 state is altered by the presence of Li, resulting in an enhanced LDOS around 2.15 eV,[33] while Stefanou et al. interpreted this peak as caused by the s-SAMO.[19] Now, we can clearly see that both interpretations are correct because both LUMO + 2 and 1s-SAMO are located in the same energy region. The presence of Li induces the overlap of the wavefunctions of Li and C_{60}, resulting in their hybridization and induced asymmetry of the 1s-SAMO. Therefore, the increased LDOS in the LUMO + 2 region as compared to C_{60}/Cu(111) is caused by the presence of Li and the respective 1s-SAMO.

Recently, it has been demonstrated that the Li position inside the C_{60} cage can be switched by STM through an inelastic scattering mechanism.[22] Therefore, it is of key importance to investigate how the Li position affects the SAMO states. Figure 2 exhibits the evolution of different SAMOs depending on the Li position inside the fullerene cage. At the equilibrium geometry, where Li resides just below the upper hexagon, the 1s-SAMO state is delocalized within the upper hemisphere with its wavefunction aligned toward the slab. However, one can expect the opposite feature when Li is located at the bottom position. Therefore, the 1s-SAMO has an asymmetrical form, the distribution of which depends on the Li position inside the C_{60} cage. Irrespective of the Li position, there is no significant wavefunction distribution of 1s-

https://doi.org/10.1021/acs.jpcc.2c02098
J. Phys. Chem. C 2022, 126, 15891−15898

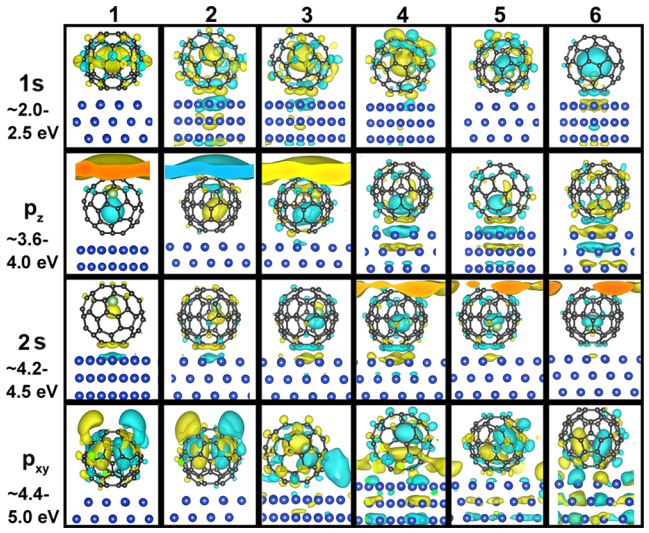

Figure 2. Wavefunction distributions of 1s-, p_z-, 2s-, and p_{xy}-SAMO states of Li@C_{60}/Cu(111). The numbers in the upper panel correspond to Li positions marked in Figure 1b.

SAMO above the molecule, and the most prominent distribution can be observed inside the C_{60} cage. The other (p_z-, 2s-, and p_{xy}-) SAMOs demonstrate clear interaction with the Cu(111) surface at some Li positions, and the wavefunctions of the nearest neighbor Li@C_{60} overlap depending on the Li position.

When Li is located in the upper part of the C_{60} cage with respect to the surface, the p_z-SAMO can be observed outside the cage (Figure 2, columns 1−3) with prominent electron density distribution overlapping with the nearest neighbor molecules, resulting in nearly free electron states.[18,20] Once the Li position changes to 4, 5, or 6 (i.e., bottom part of the cage), the p_z-SAMO starts to interact with the copper slab, resulting in a clear overlap between them. The intermediate positions exhibit distorted SAMO behavior inside the cage. In contrast, the 2s-SAMO can only be seen for those Li positions where Li resides in the bottom hemisphere of C_{60} (i.e., 4, 5, and 6) due to its nature of distribution at the opposite side of the cage. We find that in these positions, the 2s-SAMO strongly interacts with the nearest neighbors, showing that the wavefunctions overlap in intermolecular space. Therefore, the wavefunction is distributed not over the molecules like in the case of the p_z-SAMO, but between them, also resulting in delocalized states. At the same time, the upper Li locations (1, 2, and 3) lead to interaction between the 2s-SAMO and the copper slab, making it invisible for STM measurements. The p_{xy}-SAMO is located at 4.4−5.0 eV, according to our calculations, which is comparable to the region reported experimentally for Li@C_{60}/Au (111) (4.5−5.5 V) by Stefanou et al.[19] Therefore, using the state-of-art STM technique, one could expectedly switch the position of Li inside the cage[22] and observe different SAMOs experimentally.

It can be anticipated that the position of Li affects not only the wavefunction distribution but also the energy of a SAMO. For each Li position, we have plotted the projected density of states (Figure 3). The gray fillings correspond to the equilibrium state of Li, while the black lines correspond to the bottom metastable position of Li. One can see that the SAMO PDOS is significantly altered by the Li position and general behavior is the same for respective SAMO in every case. The most stable Li position results in lower SAMO energy, therefore, for such a state, the SAMO is stabilized. On comparing the PDOS plot for different positions of Li (2 and 3), a major shift in the peak is observed only for the 1s-SAMO states and, somewhat surprisingly, the PDOS plot of position 3 of Li nearly overlaps with that of position 1. A blue shift of ∼0.1−0.15 eV occurs for the bottom Li position (6) compared to that of top (1). The most prominent shift is seen for the 1s-SAMO. The intermediate Li positions lead to intermediate electronic states (between (1) and (6)). All data are well reproduced for each SAMO, and the order of the peaks correlates perfectly.

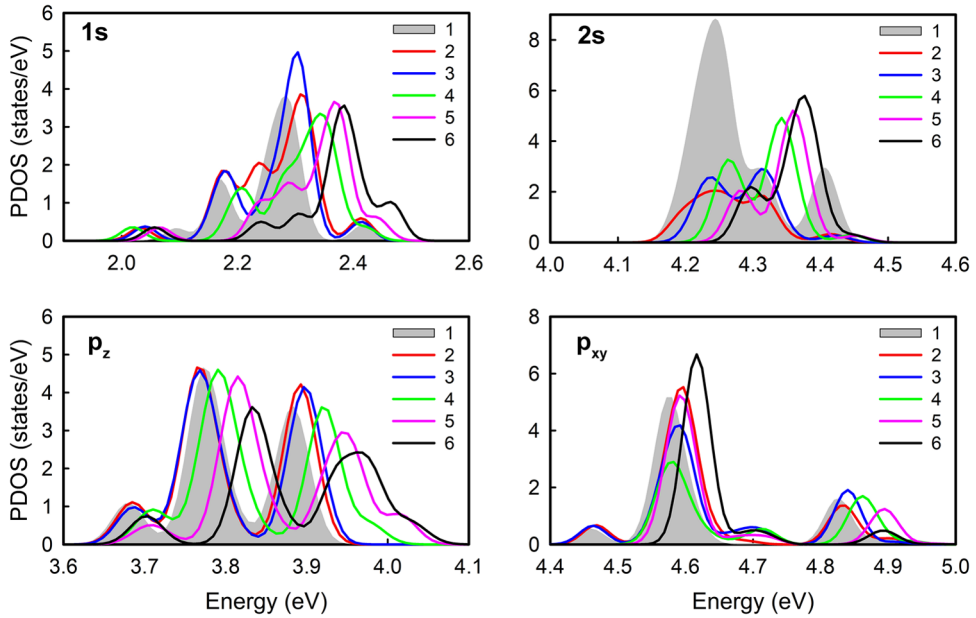

Figure 3. Projected density of states of different Li positions inside C_{60} on Cu(111) for various SAMO states. The SAMOs are listed in bold, and the numbers correspond to Li positions depicted in Figure 1b.

https://doi.org/10.1021/acs.jpcc.2c02098
J. Phys. Chem. C 2022, 126, 15891−15898

To get a deeper insight into this effect and explain the nature of SAMO shifts upon Li switching, the charge transfer to the cage from the surface and Li was analyzed using Bader charge analysis (BCA),[34] as implemented by Henkelman et al.[35,36] We could conclude that the Bader charge is well converged with reference to the current mesh—the precision of the BCA in the conservation of charge is here evaluated based on the total number of valence electrons obtained by integrating over the Bader regions. We find that at the Li(1) position, 0.06 *e* is less transferred to the cage as compared to the Li(6) position, something that is likely responsible for the small energy shift of SAMOs. We believe that the effect primarily results from Li interaction with the C_{60} cage, where a stronger overlap causes a blue shift. Although this conclusion is not very intuitive, it has indeed been demonstrated that the location of Li exactly in the center of the C_{60} cage, where the interaction with the cage is at a minimum, reveals a 0.85 eV smaller E_f—SAMO gap compared to the optimized position.[18] This confirms our assumption. It follows that effective manipulation of the endohedral position can help to achieve the desired E_f—SAMO gap.

Next, to determine the shape of single-molecule SAMO states and to reveal the interaction distance between the SAMOs, we simulate an enlarged supercell containing one Li@C_{60} molecule per 8 × 8 Cu(111) slab (Figure 4), with an intermolecular distance of 20.43 Å. This distance corresponds to one omitted C_{60} site. Figure 4a shows the most representative SAMO states. One can see that the p_z-SAMO has a clear mushroom-hat-like form for both $Li_{top}@C_{60}$ and C_{60} molecules, while the 2s-SAMO of $Li_{bottom}@C_{60}$ possesses strongly delocalized features, revealing an orbital overlap of neighboring molecules at a distance of more than 2 nm with the formation of delocalized states in the intermolecular region. The practical realization of these states could significantly enhance the conductivity of the well-ordered monolayer via the realization of the band transport. However, we should note that this state is not an equilibrium state (due to substrate-induced repulsion), and additional external stimuli are required to stabilize Li in the bottom hemisphere.

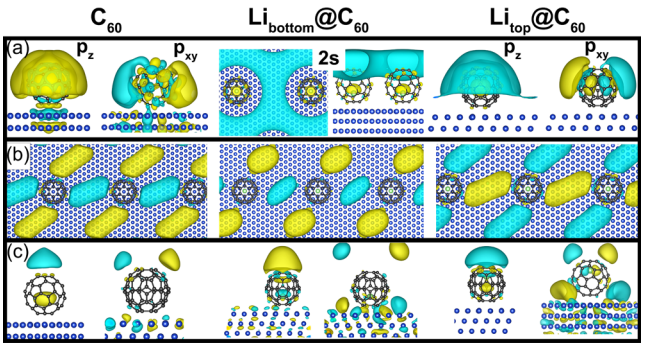

Figure 4. SAMO states of Li@C_{60} and C_{60} molecules separated by 20.43 Å on an 8 × 8 Cu(111) superstructure. (a) Selected representative SAMO states, (b) $d_{x^2-y^2,xy}$-SAMO states, and (c) d_{z^2} (left panel) and $d_{xz,yz}$ (right panel)-SAMO states.

Although most s- and p-SAMO states reveal similar shapes, we are able to identify the five d-SAMO orbitals. All of these d-SAMOs are located ∼0.3 (C_{60}) and 0.4 eV (Li@C_{60}) higher than the respective p_{xy}-SAMO and lie close to each other within an energy window of 0.15 eV. In Figure 4b, the $d_{x^2-y^2,xy}$-SAMO reveals strongly delocalized features, demonstrating a spread of these states in the intermolecular region. At the same time, the d_{z^2}- and $d_{xz,yz}$-SAMOs reveal electron distributions just above the C_{60} cage (Figure 4c). The shape of the outside distribution of the d_{z^2}-SAMO is not so strongly affected by the Li position and is always visible over the fullerene molecule with minor differences in wavefunction distribution. The plotted shape of the $d_{xz,yz}$-SAMO is in excellent agreement with previous low-temperature STM images reported by Petek and colleagues.[13]

To investigate the effect of a substrate on the SAMO states, we calculated a well-ordered Li@C_{60} monolayer on the Au(111) surface for two different positions of Li inside the cage (top and bottom, which are similar to those of the Li@C_{60} monolayer on Cu(111) surface). Several studies reported the deposition and diffusion of C_{60} on the Au(111) surface,[37,38] including the experimental findings by Gardener et al.,[39] which demonstrated highly mobile vacancies at the $C_{60}/(2\sqrt{3} \times 2\sqrt{3})$ $R30°$ Au(111) interface. Recently, Villagómez et al. reported that the most stable adsorption site of C_{60}/Au(111) is hexagonal,[40] which is similar to that of copper. However, we note that typically mixed orientations of the C_{60} cage with respect to the Au(111) surface are observed in experiments. Based on the previous information and the ability of direct comparison of the results to the Li@C_{60}/Cu(111) case, we have adopted a structure with Li encapsulated C_{60} on the $(2\sqrt{3} \times 2\sqrt{3})$ $R30°$ surface of Au(111) with a hexagonal orientation of C_{60} toward the surface to study the super atomic molecular orbitals. The lattice parameter of the $(2\sqrt{3} \times 2\sqrt{3})$ $R30°$ Au(111) surface equals 9.96 Å, which is ∼3% smaller as compared to that of 4 × 4 Cu(111). Therefore, fullerenes are placed a bit closer to each

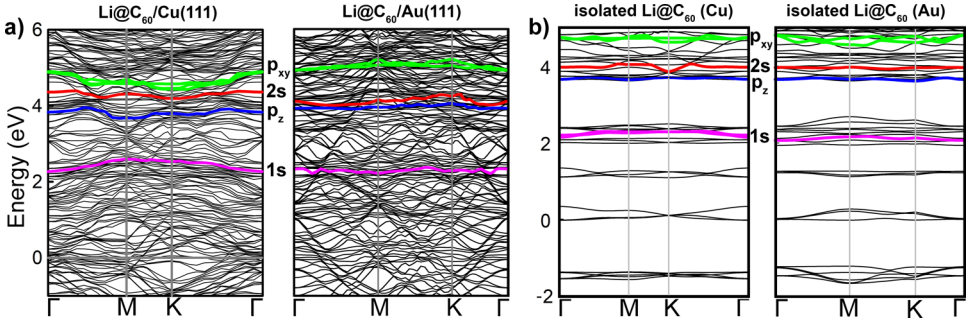

Figure 5. Band structures of (a) Li@C_{60}/Cu(111) and Li@C_{60}/Au(111) and (b) isolated single-layer (SL) Li@C_{60} with the same lattice parameter like on the copper (left panel) and gold (right panel) surfaces. The 1s-, p_z-, 2s-, and p_{xy}-SAMOs are indicated by pink, blue, red, and green lines, respectively. The Fermi levels are set to 0 eV.

https://doi.org/10.1021/acs.jpcc.2c02098
J. Phys. Chem. C 2022, 126, 15891−15898

other, resulting in a stronger overlap between them. We found that the spatial electron density distributions of the delocalized SAMO states in the case of Li@C_{60}/Au(111) are similar to those of our previous findings for the Cu(111) surface. The s-SAMO is delocalized within the cage, whereas the p_z and p_{xy} SAMOs are both inside and outside the cage, similar to the case of copper.

To demonstrate how the SAMO states are affected by the substrate, we calculated the band structures of the Li@C_{60}/Cu(111), Li@C_{60}/Au(111) heterostructures, and isolated single-layer (SL) Li@C_{60}, as shown in Figure 5. The band structures of the isolated monolayers (Figure 5b) are similar to the one previously reported in ref 18. The minor difference in p_{xy}-SAMO can be assigned to the use of the same cell parameter as for Li@C_{60} on Cu(111) and on Au(111) in the current research but could be different from that in the relaxed monolayer. The monolayer−substrate-induced interaction results in changes in the band dispersion of all SAMOs (Figure 5a). As compared to the isolated Li@C_{60} monolayer, the SAMO band dispersion becomes stronger in part of the momentum space in the case of Li@C_{60}/Cu(111). It could be noted that in the Li@C_{60}/Cu(111) heterostructure, 1s-SAMO has a positive dispersion, whereas p_z and 2s show very flat and sometimes a negative dispersion. This can be explained by strong interaction with the copper substrate and, as a result, significant charge transfer, which affects the band dispersion. Especially, this can be seen in the difference between the SAMO dispersion in Li@C_{60}/Cu(111) and Li@C_{60}/Au(111), which can be assigned to the different charge transfers from the substrate and to different Li@C_{60} intermolecular distances. The charge transferred from the substrate in Li@C_{60}/Cu(111) induces wider SAMO band dispersions, while for the minor charge transfer in Li@C_{60}/Au(111), the SAMO band widths are more or less preserved, similar to isolated monolayers. At the same time, one can observe a negligible amount of change in the energies of the SAMOs with respect to the Fermi level between Li@C_{60}/Cu(111) and Li@C_{60}/Au(111). However, the energies are comparable, indicating an insignificant effect of the substrate on the shift of the SAMO band energy.

To make the study more systemic, we additionally calculated the band structure of Li@C_{60} on the Ag(111) surface (Figure S1), which has a similar lattice to Au(111). One can see that the trend on energies of SAMO bands is similar to that of Li@C_{60} on Cu(111) and Au(111) surfaces. The charge transferred from the Ag(111) surface to the cage (0.42 e) is larger compared to that transferred from Au(111) (0.034 e), inducing wider SAMO band dispersions as compared to Au(111).

It should be noted that a real C_{60}/Cu(111) interface can demonstrate the reconstruction of the copper surface revealed in nanopits.[41−43] Such a kind of reconstruction represents removing part of the top copper layer, forming cavities on the surface where fullerenes can reside. Because more carbon atoms directly interact with copper atoms in this configuration, it is expected that more pronounced charge transfer should take place. Indeed, it was previously demonstrated that up to three electrons can be transferred to C_{60} due to a reconstructed interface with ordered seven-atom vacancy holes in the surface.[42] Thus, we carried out electronic structure calculations of Li@C_{60} on the Cu(111) substrate with nanopits (Li@C_{60}/$Cu(111)_{pits}$), as shown in Figures S1 and S2. The results demonstrate that charge transfer from metal to the cage reaches 1.27 e. This value is twice larger compared to charge transfer in unreconstructed Li@C_{60}/Cu(111). In this case, the dispersion width of the higher-lying p_{xy}-SAMO is found to be altered. Here, we would like to note that our theoretical data on unreconstructed Li@C_{60}/Cu(111) is also in fair agreement with recent experimental observation in terms of SAMO energies as well as STM images for 1s- and p_z-SAMOs.[20] It is also clear that SAMO band dispersion strictly depends on the support.

The dispersion of SAMO states suggests that there is a correlation between the nature of a substrate and the SAMO band width. In the case of Cu(111) and $Cu(111)_{pits}$, p-SAMOs are mostly affected, while for Ag(111), s-SAMOs are mostly altered. Therefore, we believe that substrate states in certain energy regions hybridize with Li@C_{60}, affecting the dispersion of certain bands. At the same time, heterostructures of Li@C_{60} and a substrate with weak binding preserve a very similar band dispersion to that of the isolated monolayer.

As SAMO states are beneficial for transport applications and reveal delocalized electron density, it is required to calculate effective masses of low-lying s- and p_z-SAMO bands to have some estimation of the transport properties. Therefore, effective masses are calculated for Li@C_{60} on Cu(111) and also for the isolated monolayer to highlight changes that take place due to the substrate. Effective masses are evaluated numerically by the second-order polynomial fitting of the calculated band dispersion curves around the high-symmetry points with low-lying states (Table 1). The calculated effective masses for the s-SAMO are compared to the p_z-SAMO similarly to C_{60}.[18] By comparing the effective masses of the free-standing Li@C_{60} layer and Li@C_{60}/Cu(111), obviously, the interaction of Li@C_{60} with the Cu(111) substrate is beneficial for the SAMOs, making the respective band dispersion steeper, therefore affecting transport properties. The present results are qualitatively similar to those reported previously for isolated 2D Li@C_{60}.[18] However the effective masses found in the present work are a bit lower compared to the previously reported ones. In addition, we demonstrate that the carrier mobility of the p_z-SAMO of Li@C_{60} should be calculated in a highly symmetrical M-point instead of the Γ-point because the respective band dispersion possesses the lowest energy in the M-point (Figure 5) and it has not been considered previously. The complete band structure was also yet to be reported until the present work.

Table 1. Effective Masses (in $m_0 = 9.11 \times 10^{-31}$ kg) of SAMO Bands for 2D Li@C_{60}

	Li@C_{60}	Li@C_{60}/Cu(111)	Li@C_{60}[a]
s-SAMO	1.4(Γ)	0.7(Γ)	1.5
p_z-SAMO	1.1(Γ), 0.8(M)	0.9(Γ), 0.4(M)	1.2

[a]Results were taken from ref 18.

To validate our results, we also calculated effective masses of s- and p_z-SAMO bands of the C_{60} monolayer without Li doping (Table S1). The calculated effective mass of s-SAMO equals 0.7 m_e for a lattice constant of 4 × 4 Cu(111) (a = 10.26 Å), while effective masses of p_z-SAMO are 0.9 and 0.4 m_e for the band dispersion fitted in Γ- and K-points, respectively. We find that these results are in qualitative agreement with the previously reported ones,[18] although the effective masses may be underestimated. It is clearly seen that, with Li doping, the wavefunction of s-SAMO becomes localized, and the band becomes flat in the Γ-point.

https://doi.org/10.1021/acs.jpcc.2c02098
J. Phys. Chem. C 2022, 126, 15891−15898

It is important to compare the effective masses of the free-standing Li@C_{60} (C_{60}) layers and those on the Cu(111) substrate (Li@C_{60} (C_{60})/Cu(111)). For both cases of Li@C_{60}/Cu(111) and C_{60}/Cu(111), the monolayer with the Cu(111) substrate shows a reduced effective mass of both s-SAMO and p_z-SAMO. The detail of the change in the s-SAMO band near the Γ-point is shown in Figure S3. Note that the lattice parameter for the Li@C_{60} (C_{60}) monolayer is the same as on the substrate. Therefore, the difference in the effective mass should be only due to the presence of the substrate. Although this effect of the substrate on the dispersion of the SAMO bands is quite important to control the SAMOs of the C_{60} films, the mechanism behind this effect should be profound. For example, Figure S1 shows that in the case of Li@C_{60}/Ag(111), a significant effect is seen in 2s-SAMO, and, in the case of Li@C_{60}/Cu(111) with the pit structure in the top layer of the substrate, p_{xy}-SAMO is affected. Therefore, the SAMO dispersion is rather sensitive to the electronic states at the interface, and a detailed understanding of their relationship will be necessary for the manipulation of the SAMO bands.

There are two important reports on the Li@C_{60}/Au(111) interface revealing that the p_z-SAMO lies below the 1s-SAMO[19,22] This could be the basis for realizing practical applications. However, such an order is not intuitive because normally, these orbitals have reverse order and are well separated (∼1.6 eV) for Li@C_{60} monolayers with and without Cu(111) support. We do not expect that a relatively inert Au(111) surface can induce such a drastic change in SAMO states. Figure 6 demonstrates that the PDOS peaks for 1s-, p_z-, and p_{xy}-SAMOs are very similar to that of the Cu(111) case and are found to be 2.0−2.4, 3.7−4.1, and 4.8−5.2 eV. Comparing the DOS plots between Li@C_{60}/Cu and Li@C_{60}/Au (Figures 1c and 6), one can find that the SAMOs of Li@C_{60}/Cu have wider peaks than those on the Au substrate, which is related to the difference in intermolecular distances and charge transfer from the respected substrate. In comparison with our previous results for Li@C_{60} on a Cu(111) surface, a small shift of about 0.3 eV to higher energies is seen for the p_{xy}-SAMO. The difference in the energy between the Cu and Au substrates can also be related to the intermolecular distance of the respective fullerene monolayer, resulting in different crystal field effects. Therefore, the reported p_z-SAMO of Li@C_{60}/Au(111) at ∼1.5 eV by M Stefanou et al.[19] and ∼1 eV by Chandler et al.[22] was likely assigned to the LUMO + 1 state, while LUMO + 2 was assigned to the LUMO + 3 region. We believe that the comparison of STM results with the results of PBC calculations is more reasonable due to the fact that a more realistic model is employed, including interactions with the surface and nearest neighbors. We have additionally carried out Li@C_{60}/Cu(111) calculations with the hybrid HSE06 functional[44] to verify that our results were not affected by the theory level and found the same SAMO order with some energy shift compared to PBE. This once again confirms our results and demonstrates that SAMO order is not sensitive to functionals.

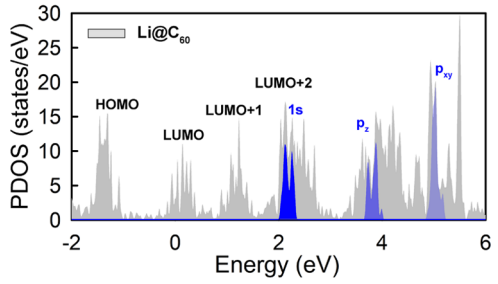

Figure 6. Calculated projected density of states (DOS) of s- and p-SAMO states for Li@C_{60}/Au(111). The SAMOs are multiplied by a factor of 3. The Fermi level is set to 0 eV.

Furthermore, the charge transfer to the cage from the surface and Li (top) is calculated using Bader charge analysis to determine the effect of the substrate on the SAMO states. The net charge of the C_{60} cage is observed to be −0.93 *e*, indicating that the charge is acquired from Li and the Au(111) surface. The amount of charge transferred from the Li atom to the C_{60} cage (0.899 *e*) is comparable to that of Li@C_{60}/Cu(111), whereas a very small amount of charge (0.034 *e*) is transferred from Au(111) to the cage which confirms the absence of covalent bonding between the surface and the C_{60} cage. This also explains the nonuniform orientation of the C_{60} cage with respect to the Au(111) surface found in many experimental observations in contrast to the Cu(111) surface, where all of the deposited molecules are well-ordered within an island. The amount of charge transfer from the substrate to the cage is found to be 0.015 *e* in the case of the bottom position of Li inside the cage which confirms that the top position of Li is more energetically favorable than the other positions. Indeed, the energy difference between the different positions of Li inside the cage is negligible compared to that of the Cu(111) surface, and the top position is found 0.06 eV more favorable compared to the bottom one. Therefore, the confinement of Li is not as strong as in the case of Cu(111). [20] This also shows that there is a significant difference in the stability of the p_z-, 2s-, and p_{xy}-SAMOs of Li@C_{60} on different substrates. We expect that Li will be rather delocalized in Li@C_{60}/Au(111) and therefore that this could result in difficulties with the formation and experimental determination of the delocalized SAMO bands.

The above comparison results in the important conclusion that the dispersion of SAMO states depends on the amount of charge transferred from the substrate, while it cannot provide any sizable effect on the energies of low-lying SAMO states. The realization of the C_{60} monolayer on a phosphorene surface[45] also did not demonstrate any sizable effect on the SAMO level doping that confirms our assumption. Therefore, the nature of the fullerene itself and endohedral doping are primarily responsible for the SAMO energy.

CONCLUSIONS

Based on first-principles calculations, we systematically investigated the evolution of superatom molecular orbitals in Li@C_{60} on different substrates and with respect to different Li^+ positions. We demonstrated that changing Li coordination inside the C_{60} cage leads to a significant alteration of SAMO wave functions and changes in the SAMO electronic structure. The equilibrium Li position under the top hexagon of C_{60} reveals the lowest SAMO energies for all superatom molecular orbitals. The electronic structure calculations demonstrate a minor substrate effect for the SAMO energies but also that a substrate causes a noticeable change in the SAMO band dispersion through the charge transfer and the modification of the intermolecular distance and confinement of Li. This reflects the molecule−substrate interaction and the electron transfer at the interface. Therefore, although the substrate

https://doi.org/10.1021/acs.jpcc.2c02098
J. Phys. Chem. C 2022, 126, 15891−15898

effects are still comparatively small, a substrate must be correctly selected to form a well-ordered Li@C_{60} monolayer important for the creation of delocalized nearly free electron states. Further exploration of the nature, or selection, of the fullerene itself and endohedral doping is required to push the SAMO energies close to the Fermi level and therefore make Li@C_{60} suitable for practical application. We believe that our results can provide a useful step in further engineering of superatom molecular orbitals.

■ ASSOCIATED CONTENT

Supporting Information

The Supporting Information is available free of charge at https://pubs.acs.org/doi/10.1021/acs.jpcc.2c02098.

Band structures of Li@C_{60}/Ag(111) and Li@C_{60}/Cu(111) with nanopits (Figure S1); top view of Li@C_{60}/Cu(111) pits heterostructure with six-atoms pits in the top copper layer (Figure S2); comparative s-SAMO band distribution of C_{60}/Cu(111), C_{60}, Li@C_{60}, and Li@C_{60}/Cu(111) in the vicinity of the Γ-point (Figure S3); effective masses of SAMO bands for 2D C_{60} (Table S1) (PDF)

■ AUTHOR INFORMATION

Corresponding Authors

Artem V. Kuklin − *Department of Physics and Astronomy, Uppsala University, SE-751 20 Uppsala, Sweden;* orcid.org/0000-0002-9371-6213; Email: artem.icm@gmail.com

Yoichi Yamada − *Faculty of Pure and Applied Sciences, R&D Center for Innovative Material Characterization, University of Tsukuba, Tsukuba, Ibaraki 305-8577, Japan;* orcid.org/0000-0001-8187-3409; Email: yamada@bk.tsukuba.ac.jp

Authors

Rahul Suresh − *International Research Center of Spectroscopy and Quantum Chemistry—IRC SQC, Siberian Federal University, 660041 Krasnoyarsk, Russia*

Konoha Shimizu − *Faculty of Pure and Applied Sciences, R&D Center for Innovative Material Characterization, University of Tsukuba, Tsukuba, Ibaraki 305-8577, Japan*

Hans Ågren − *Department of Physics and Astronomy, Uppsala University, SE-751 20 Uppsala, Sweden;* orcid.org/0000-0002-1763-9383

Complete contact information is available at: https://pubs.acs.org/10.1021/acs.jpcc.2c02098

Notes

The authors declare no competing financial interest.

■ ACKNOWLEDGMENTS

R.S. acknowledges the support of the Russian Science Foundation (Project 19-73-10015). This work was also supported by the Olle Engkvist Byggmästare Foundation (contract no. 212-0178), JSPS KAKENHI Grant Numbers 20H02808 and 19K05182, and partly performed under the approval of the Photon Factory Program Advisory Committee (2018S2-005) and UVSOR (20-260). The authors thank the Swedish National Infrastructure for Computing (SNIC 2021-3-22) at the National Supercomputer Centre of Linköping University (Sweden), partially funded by the Swedish Research Council through grant agreement no. SNIC 2021/3-22 and 2021/6-335.

■ REFERENCES

(1) Kroto, H. W.; Heath, J. R.; O'Brien, S. C.; Curl, R. F.; Smalley, R. E. C_{60}: Buckminsterfullerene. *Nature* **1985**, *318*, 162−163.

(2) Hebard, A. F.; Rosseinsky, M. J.; Haddon, R. C.; Murphy, D. W.; Glarum, S. H.; Palstra, T. T. M.; Ramirez, A. P.; Kortan, A. R. Superconductivity at 18 K in Potassium-Doped C_{60}. *Nature* **1991**, *350*, 600−601.

(3) Heath, J. R.; O'Brien, S. C.; Zhang, Q.; Liu, Y.; Curl, R. F.; Tittel, F. K.; Smalley, R. E. Lanthanum Complexes of Spheroidal Carbon Shells. *J. Am. Chem. Soc.* **1985**, *107*, 7779−7780.

(4) Bethune, D. S.; Johnson, R. D.; Salem, J. R.; de Vries, M. S.; Yannoni, C. S. Atoms in Carbon Cages: The Structure and Properties of Endohedral Fullerenes. *Nature* **1993**, *366*, 123−128.

(5) Olmstead, M. M.; de Bettencourt-Dias, A.; Duchamp, J. C.; Stevenson, S.; Marciu, D.; Dorn, H. C.; Balch, A. L. Isolation and Structural Characterization of the Endohedral Fullerene $Sc_3N@C_{78}$. *Angew. Chem., Int. Ed.* **2001**, *40*, 1223−1225.

(6) Wang, C.-R.; Kai, T.; Tomiyama, T.; Yoshida, T.; Kobayashi, Y.; Nishibori, E.; Takata, M.; Sakata, M.; Shinohara, H. A Scandium Carbide Endohedral Metallofullerene: $(Sc_2C_2)@C_{84}$. *Angew. Chem., Int. Ed.* **2001**, *40*, 397−399.

(7) Popov, A. A.; Yang, S.; Dunsch, L. Endohedral Fullerenes. *Chem. Rev.* **2013**, *113*, 5989−6113.

(8) Ohno, K.; Maruyama, Y.; Esfarjani, K.; Kawazoe, Y.; Sato, N.; Hatakeyama, R.; Hirata, T.; Niwano, M. Ab Initio Molecular Dynamics Simulations for Collision between C_{60} and Alkali-Metal Ions: A Possibility of Li@C_{60}. *Phys. Rev. Lett.* **1996**, *76*, 3590.

(9) Wan, Z.; Christian, J. F.; Anderson, S. L. Collision of Li^+ and Na^+ with C_{60}: Insertion, fragmentation, and thermionic emission. *Phys. Rev. Lett.* **1992**, *69*, 1352.

(10) Tellgmann, R.; Krawez, N.; Lin, S.-H.; Hertel, I. V.; Campbell, E. E. B. Endohedral Fullerene Production. *Nature* **1996**, *382*, 407−408.

(11) Martins, J. L.; Troullier, N.; Weaver, J. H. Analysis of Occupied and Empty Electronic States of C_{60}. *Chem. Phys. Lett.* **1991**, *180*, 457−460.

(12) Jost, M. B.; Troullier, N.; Poirier, D. M.; Martins, J. L.; Weaver, J. H.; Chibante, L. P. F.; Smalley, R. E. Band Dispersion and Empty Electronic States in Solid C_{60}: Inverse Photoemission and Theory. *Phys. Rev. B* **1991**, *44*, 1966−1969.

(13) Feng, M.; Zhao, J.; Petek, H. Atomlike, Hollow-Core − Bound Molecular Orbitals of C_{60}. *Science* **2008**, *320*, 359−363.

(14) Dutton, G. J.; Dougherty, D. B.; Jin, W.; Reutt-Robey, J. E.; Robey, S. W. Superatom Orbitals of C_{60} on Ag(111): Two-Photon Photoemission and Scanning Tunneling Spectroscopy. *Phys. Rev. B* **2011**, *84*, No. 195435.

(15) Shibuta, M.; Yamamoto, K.; Guo, H.; Zhao, J.; Nakajima, A. Highly Dispersive Nearly Free Electron Bands at a 2D-Assembled C_{60} Monolayer. *J. Phys. Chem. C* **2020**, *124*, 734−741.

(16) Pavlyukh, Y.; Berakdar, J. Communication: Superatom Molecular Orbitals: New Types of Long-Lived Electronic States. *J. Chem. Phys.* **2011**, *135*, No. 201103.

(17) Guo, H.; Zhao, C.; Zheng, Q.; Lan, Z.; Prezhdo, O. V.; Saidi, W. A.; Zhao, J. Superatom Molecular Orbital as an Interfacial Charge Separation State. *J. Phys. Chem. Lett.* **2018**, *9*, 3485−3490.

(18) Zhao, J.; Feng, M.; Yang, J.; Petek, H. The Superatom States of Fullerenes and Their Hybridization into the Nearly Free Electron Bands of Fullerites. *ACS Nano* **2009**, *3*, 853−864.

(19) Stefanou, M.; Chandler, H. J.; Mignolet, B.; Williams, E.; Nanoh, S. A.; Thompson, J. O. F.; Remacle, F.; Schaub, R.; Campbell, E. E. B. Angle-Resolved Photoelectron Spectroscopy and Scanning Tunnelling Spectroscopy Studies of the Endohedral Fullerene Li@C_{60}. *Nanoscale* **2019**, *11*, 2668−2678.

(20) Sumi, N.; Kuklin, A. V.; Ueno, H.; Okada, H.; Ogawa, T.; Kawachi, K.; Kasama, Y.; Sasaki, M.; Avramov, P. V.; Ågren, H.; Yamada, Y. Direct Visualization of Nearly Free Electron States

Formed by Superatom Molecular Orbitals in a Li@C_{60} Monolayer. *J. Phys. Chem. Lett.* **2021**, *12*, 7812−7817.
(21) Ueno, H.; Jeon, I.; Lin, H.; Thote, A.; Nakagawa, T.; Okada, H.; Izawa, S.; Hiramoto, M.; Daiguji, H.; Maruyama, S.; Matsuo, Y. Li@C_{60} Endohedral Fullerene as a Supraatomic Dopant for C_{60} Electron-Transporting Layers Promoting the Efficiency of Perovskite Solar Cells. *Chem. Commun.* **2019**, *55*, 11837−11839.
(22) Chandler, H. J.; Stefanou, M.; Campbell, E. E. B.; Schaub, R. Li@C_{60} as a Multi-State Molecular Switch. *Nat. Commun.* **2019**, *10*, No. 2283.
(23) Feng, M.; Zhao, J.; Huang, T.; Zhu, X.; Petek, H. The Electronic Properties of Superatom States of Hollow Molecules. *Acc. Chem. Res.* **2011**, *44*, 360−368.
(24) Grimme, S. Semiempirical GGA-Type Density Functional Constructed with a Long-Range Dispersion Correction. *J. Comput. Chem.* **2006**, *27*, 1787−1799.
(25) Perdew, J. P.; Burke, K.; Ernzerhof, M. Generalized Gradient Approximation Made Simple. *Phys. Rev. Lett.* **1996**, *77*, 3865−3868.
(26) Kresse, G.; Furthmüller, J. Efficient Iterative Schemes for Ab Initio Total-Energy Calculations Using a Plane-Wave Basis Set. *Phys. Rev. B* **1996**, *54*, 11169−11186.
(27) Kresse, G.; Hafner, J. Ab Initio Molecular Dynamics for Liquid Metals. *Phys. Rev. B* **1993**, *47*, 558−561.
(28) Blöchl, P. E. Projector Augmented-Wave Method. *Phys. Rev. B* **1994**, *50*, 17953−17979.
(29) Monkhorst, H. J.; Pack, J. D. Special Points for Brillouin-Zone Integrations. *Phys. Rev. B* **1976**, *13*, 5188−5192.
(30) Momma, K.; Izumi, F. VESTA 3 for Three-Dimensional Visualization of Crystal, Volumetric and Morphology Data. *J. Appl. Crystallogr.* **2011**, *44*, 1272−1276.
(31) Wang, V.; Xu, N.; Liu, J. C.; Tang, G.; Geng, W.-T. VASPKIT: A user-friendly interface facilitating high-throughput computing and analysis using VASP code. *Comput. Phys. Commun.* **2019**, *267*, No. 108033.
(32) Suh, I.-K.; Ohta, H.; Waseda, Y. High-Temperature Thermal Expansion of Six Metallic Elements Measured by Dilatation Method and X-ray Diffraction. *J. Mater. Sci.* **1988**, *23*, 757−760.
(33) Yamada, Y.; Kuklin, A. V.; Sato, S.; Esaka, F.; Sumi, N.; Zhang, C.; Sasaki, M.; Kwon, E.; Kasama, Y.; Avramov, P. V.; Sakai, S. Electronic Structure of Li^+@C_{60}: Photoelectron Spectroscopy of the Li^+@C_{60}[PF_6^-] Salt and STM of the Single Li^+@C_{60}molecules on Cu(111). *Carbon* **2018**, *133*, 23−30.
(34) Bader, R. F. W. A Quantum Theory of Molecular Structure and Its Applications. *Chem. Rev.* **1991**, *91*, 893−928.
(35) Henkelman, G.; Arnaldsson, A.; Jónsson, H. A Fast and Robust Algorithm for Bader Decomposition of Charge Density. *Comput. Mater. Sci.* **2006**, *36*, 354−360.
(36) Tang, W.; Sanville, E.; Henkelman, G. A Grid-Based Bader Analysis Algorithm without Lattice Bias. *J. Phys.: Condens. Matter* **2009**, *21*, No. 084204.
(37) Paßens, M.; Waser, R.; Karthäuser, S. Enhanced Fullerene−Au(111) Coupling in $(2\sqrt{3} \times 2\sqrt{3})$R30° Superstructures with Intermolecular Interactions. *Beilstein J. Nanotechnol.* **2015**, *6*, 1421−1431.
(38) Guo, S.; Fogarty, D. P.; Nagel, P. M.; Kandel, S. A. Thermal Diffusion of C_{60} Molecules and Clusters on Au(111). *J. Phys. Chem. B* **2004**, *108*, 14074−14081.
(39) Gardener, J. A.; Briggs, G. A. D.; Castell, M. R. Scanning tunneling microscopy studies of C_{60} monolayers on Au(111). *Phys. Rev. B* **2009**, *80*, No. 235434.
(40) Villagómez, C. J.; Garzón, I. L.; Paz-Borbón, L. O. A First-Principles DFT Dispersion-Corrected C_{60}/Au(111) Raman Study. *Comput. Mater. Sci.* **2020**, *171*, No. 109208.
(41) Forcieri, L.; Taylor, S.; Moriarty, P.; Jarvis, S. P. Origin of C_{60} Surface Reconstruction Resolved by Atomic Force Microscopy. *Phys. Rev. B* **2021**, *104*, No. 205428.
(42) Pai, W. W.; Jeng, H. T.; Cheng, C. M.; Lin, C. H.; Xiao, X.; Zhao, A.; Zhang, X.; Xu, G.; Shi, X. Q.; Van Hove, M. A.; et al. Optimal Electron Doping of a C_{60} Monolayer on Cu(111) via Interface Reconstruction. *Phys. Rev. Lett.* **2010**, *104*, No. 036103.
(43) Xu, G.; Shi, X. Q.; Zhang, R. Q.; Pai, W. W.; Jeng, H. T.; Van Hove, M. A. Detailed Low-Energy Electron Diffraction Analysis of the (4 × 4) Surface Structure of C_{60} on Cu(111): Seven-Atom-Vacancy Reconstruction. *Phys. Rev. B.* **2012**, *86*, No. 075419.
(44) Heyd, J.; Scuseria, G. E.; Ernzerhof, M. Hybrid Functionals Based on a Screened Coulomb Potential. *J. Chem. Phys.* **2003**, *118*, 8207.
(45) Cui, X.; Han, D.; Guo, H.; Zhou, L.; Qiao, J.; Liu, Q.; Cui, Z.; Li, Y.; Lin, C.; Cao, L.; et al. Realizing Nearly-Free-Electron like Conduction Band in a Molecular Film through Mediating Intermolecular van Der Waals Interactions. *Nat. Commun.* **2019**, *10*, No. 3374.

https://doi.org/10.1021/acs.jpcc.2c02098
J. Phys. Chem. C 2022, 126, 15891−15898